

## ROBUST SEMI-DETERMINISTIC FACET MODEL FOR FAST ESTIMATION ON EM SCATTERING FROM OCEAN-LIKE SURFACE

H. Chen, M. Zhang, and D. Nie

School of Science  
Xidian University  
Xi'an 710071, China

H.-C. Yin

National Electromagnetic Scattering Laboratory  
Beijing 100854, China

**Abstract**—A robust semi-deterministic facet model for the computation of the radar scattering cross section from the ocean-like surface is presented. As a facet-based theory, it is a more comprehensive model which can reflect the specular and diffuse configurations, as well as the mono- and bistatic features. Significant computational efficiency and good agreement with experimental data are observed, which makes the proposed facet model well suitable for fast estimation on EM scattering and synthetic aperture radar (SAR) imagery simulation of marine scene.

### 1. INTRODUCTION

Monographic study on microwave remote sensing of the ocean is an old but vigorous research realm. With the rapid development of satellite technology, which is employed for gathering information about the terrestrial or extraterrestrial and leads to the possibility of using spacecraft in remote sensing of oceanographic parameters, more and more applications to monitor ocean environment, especially as ocean synthetic aperture radar (SAR) [1–3], have been exploited during recent years. To implement these applications, a clear and comprehensive investigation on the physical processes between the electromagnetic waves and ocean surface is desirable. Approximate models, for instance, the two classical surface scattering theories:

---

Corresponding author: M. Zhang (mzhang@mail.xidian.edu.cn).

Kirchhoff approximation (KA) [4] and Small perturbation method (SPM) [5], and many unified theories like the two scale model (TSM) [6], small-slope approximation (SSA) [7], improved Green's function method (IGFM) [8], extended boundary condition method (EBCM) [9] and integral equation method (IEM) [10], have been discussed with application to sea scatter modeling. Many of the methods mentioned above more or less meet the possible limitation on special rigorous valid conditions, Gaussian spectrum, monostatic radar, one dimensional surface or insurmountable computational complexity.

Nevertheless, the two scale theory has always been the most popular approach since it was introduced in 1970's [11,12]. The kernel of the two scale theory is the theoretical division of the real surface with two types of irregularities: Large waves whose radius of curvature is great enough for the calculation by KA, and fine ripples where SPM could be used in scattering simulation. Then the Bragg scattering contributions of the small ripples would be tilted by the large scale components. One of the most common two-scale formulas is accomplished by Fung et al. [13], and is called by the conventional TSM here for distinction. Accordingly, they evaluate large scale tilt effect by averaging the backscattering cross section from perturbation theory over the large scale slopes' probability distribution. This is a statistical approach, which encompasses both large waves and small ripples to obtain an average of the real diffusion coefficient without a particular sea height map. Additionally, it meets two drawbacks: Firstly, it is not properly accurate at angles of incidence where specular reflection from the surface is significant (smaller than about  $20^\circ$ , in which, the computational cost is also great because of the action of the lower limit of  $-\cot \theta_i$  in the integration); Secondly, although it gives a link budget, nothing is said about the radar cross section (RCS) fluctuation resulted by the local characteristics corresponding to the deterministic profile of a special sea surface. In fact, this local fluctuation is a useful feature and desirable in ocean SAR imaging model as the SAR raw signal is the appropriate superposition of returns from each facet [14]. This demand has sprung the development of the so called "facet-based" approaches which try to break the surface into slightly rough plane facets with locally approximation and represent it as a numerical elevation map, so that the instantaneous radar returns from individual facets could be obtained in SAR imagery simulation. Comparatively overall analyses are made on this topic. Franceschetti et al. [3,14] presented a facet backscattering model in which the Kirchhoff solution in physical optics approximation is used to compute the facet's backscattering. But, in some cases the scattering properties of the facet are modeled by means of the Bragg phenomena. This pattern has not been implemented in

their code. Hasselman et al. [15] introduced a EMH (electromagnetic-hydrodynamic) two-scale model which was fully developed on the basis of the standard plane surface Bragg resonance theory, and extended to the so called "SAR two-scale model". West et al. [16] also proposed a slightly-rough facet model which includes both the first-order and second-order large-scale effects (tilt and curvature). However, the bistatic configuration of sea scattering was not concerned in all of the facet models above. Thus, a more comprehensive facet model which would adequately reflect the specular and diffuse configurations, as well as the mono- and bistatic features, is in need.

In reinvestigation on the two scale composite theories for EM scattering from ocean surface, the original Bass-Fuks formulation of the two scale model draws our sight. They seek the scattered field in the form of the sum of a zero order approximation field (reflected from the smooth surface) and a first order correction field in small perturbation parameters. And an integration over an apparently deterministic profile is involved. This deterministic integration is well suit for the extension to local facet frame. However, they only gave the monostatic scattering formula with application to Gaussian distribution seas [17, 18]. And, withal, in our opinion, their model still has poor performance in the specular zone.

In this paper, the authors fall to deriving the Bass-Fuks Two Scale Model (BFTSM) to the bistatic case firstly. Moreover, as a numerical approach, each facet is characterized locally by the corresponding simulated slope on large scale oceanic surface generated by Double Superimposition Method (DSM) [19]. The elementary radar returns from each facet are computed by a blending scheme of combining geometric optics limit of the KA (KA-GO) with Bragg components of BFTSM. Then, a facet-based summation formula of scattering coefficient is proposed by summing up returns from all the facets. The proposed model could well account the two types of scattering processes and monostatic/bistatic configurations. In addition, it also results significant computational efficiency as well as good accuracy confirmed by experimental validation.

## **2. FACET STRUCTURE OF THE OCEAN SCENE**

### **2.1. Large Scale Configuration**

Many approaches were developed to describe the electromagnetic scattering from oceanic surface. The most classical one is the two scale model, which simplifies the sea wave as a superposition of two configurations: Gravity wave configuration and capillary wave configuration. In this case, the surface spectrum is classified by gravity

wave spectrum and capillary wave spectrum, denoted by  $W_g$  and  $W_c$  respectively. The large scale structure is described by the Double Superimposition Model (DSM) [19], which describes the ocean wave fluctuating on a fixed point by many cosine wave superimpositions as follows:

$$Z_{ij}(x_i, y_j, t) = \sum_{i=1}^M \sum_{j=1}^N \sqrt{2W_g(\omega_i, \theta_j) \Delta\omega_i \Delta\theta_j} \cos(k_i x \cos \theta_j + k_i y \sin \theta_j - \omega_i t + \varepsilon_{ij}) \quad (1)$$

where  $k_i$ ,  $\omega_i$ ,  $\theta_i$  represent the wave number, circle frequency and direction angle respectively.  $\varepsilon_{ij}$  could be selected randomly between  $0 \sim 2\pi$ . On deep water,  $k_i$  and  $\omega_i$  meet the relation with  $\omega_i^2 = gk_i$ . The gravity wave spectrum  $W_g$  is chosen by JONSWAP spectrum as follows:

$$W_g(\omega, \varphi) = \varphi(\omega, \varphi) \alpha g^2 \frac{1}{\omega^5} \exp \left[ -\frac{5}{4} \left( \frac{\omega_m}{\omega} \right)^4 \right] \cdot \gamma \exp \left[ -\frac{(\omega - \omega_m)^2}{2\sigma^2 \omega_m^2} \right] \quad (2)$$

$\varphi(\omega, \varphi)$  is the spreading function proposed by Stereo Wave Observation Project:

$$\varphi(\omega, \phi) = (1 + p \cos 2\phi + q \cos 4\phi) / \pi, \quad |\theta| \leq \pi/2 \quad (3)$$

$p = 0.50 + 0.82 \exp[-0.5(\omega/\omega_m)^4]$ ,  $q = 0.32 \exp[-0.5(\omega/\omega_m)^4]$ ,  $\gamma$  is the peak enhancement factor,  $\sigma$  is the peak width parameter,  $\omega_m$  is the frequency of the spectral peak,  $\omega_m = 22g\tilde{x}^{-0.33}/u$ ,  $\tilde{x} = gx/U^2$  ( $x$  is the wind fetch,  $U$  is the wind speed at 10 m above the mean sea level).

The large scale slope distribution of rough sea profile plays an important role on oceanic microwave scattering calculations. In many of the surface scattering theories available, the probability density distribution of sea slope is described as Gaussian or Weibull distribution. However, based on the observation data, Cox and Munk stated that the distribution of sea slope owns non-Gaussian features. They presented the probability density function of large-scale sea slope distribution function, so called Cox-Munk PDF [20].

In this work, we seek the large-scale slope matrixes along  $x$  or  $y$  directions on the basis of the generated sea height map and denote them by  $[\alpha_{i,j}]_{M \times N}$  and  $[\beta_{i,j}]_{M \times N}$  respectively, where  $\alpha_{i,j} = \partial Z_{i,j} / \partial x$ ,  $\beta_{i,j} = \partial Z_{i,j} / \partial y$ . The slope distributions along  $x$  and  $y$  direction of generated two-dimensional rough sea surface are displayed in Fig. 1. Two main observations may be found: (1) When the wind direction is chosen to be along  $x$ -axis (downwind), a greater width and lower peak value occurring as the ocean becomes rougher with wind speed would be found. A comparison is also made between the simulated sea

slope PDF and Cox-Munk PDF. It shows that they are comparatively consistent with each other (see in Figs. 1(a) and (b) in detail). The difference between the PDF and computational result becomes larger in Fig. 1(b). This slight inconsistency may be caused by the linear superimposition simplification of the sea waves as described in DSM. The slopes along  $x$ -direction could be reflected sufficiently when the down wind blows along  $x$ -axis. While in  $y$ -direction, equivalently to cross wind, the simulated wave develops insufficiently. A non-linear process of the wave interaction should be introduced to improve this issue. However, due to the simulation efficiency, this is not concerned here. (2) When the wind speed is fixed at 5 m/s, the variations with the wind direction is investigated in Figs. 1(c) and (d). Since the wind direction is chosen to be along the  $x$ -axis (downwind), the sea surface has more roughness along  $x$ -direction than along  $y$ -direction. Hence this leads to the narrower width and higher peak of curves along  $y$ -direction than along  $x$ -direction. While in crosswind direction, it reverses. (Also see in Figs. 1(c) and (d)) The logical results above indicate that the mentioned numerical method used to simulate the

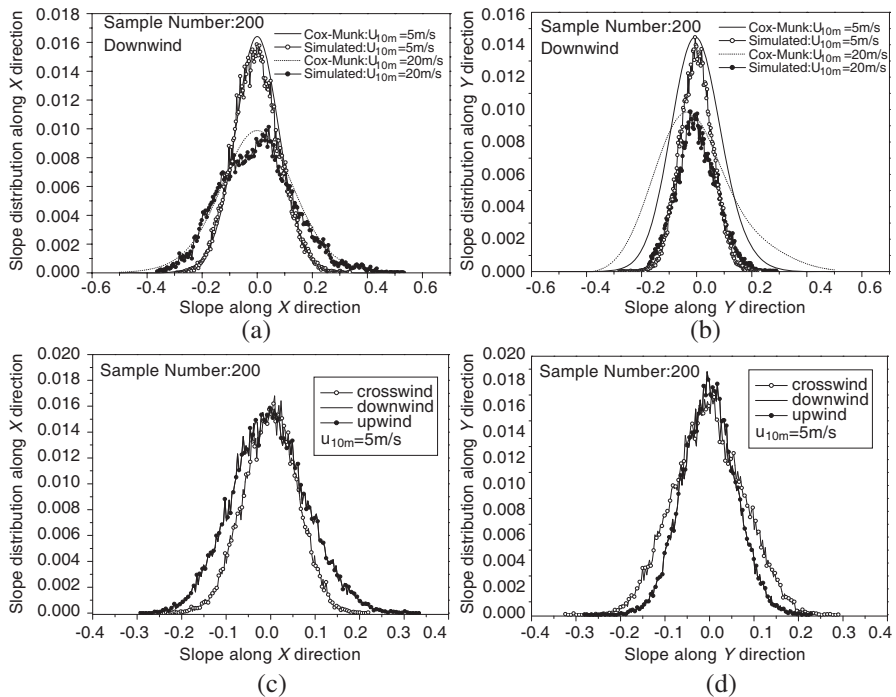


Figure 1. Simulation of large-scale sea slopes.

large-scale sea slope is feasible.

### 2.2. Small Scale Configuration

The small surface is described by the capillary spectrum  $W_c(K)$ , and adapted to the real surface by a tilting process with large scale slopes. We chose the  $W_c(K)$  as the Pierson’s capillary spectrum:

$$W_c(K, \varphi) = W_c(k)S(k, \varphi) \tag{4}$$

where

$$S(k, \varphi) = a_0 + a_1 \left( 1 - e^{-bk^2} \right) \cos 2\varphi$$

$$W_c(k) = 0.875 \cdot (2\pi)^{p-1} \cdot (1 + 3k^2/k_m^2) g^{(1-p)/2} [k (1 + k^2/k_m^2)]^{-(p+1)/2}$$

Detail information for each parameter above could be found in Ref. [13].

## 3. FACET SCATTERING MODEL

### 3.1. Bistatic Investigation on Bass-fuks Two Scale Model (BFTSM)

The interest in bistatic radar application has rapidly increased in recent years. Bistatic radar can offer extra information which is not available from the monostatic case because of the different two-way observation geometry. For instance, for objects that show a low RCS in monostatic directions, one can find suitable bistatic angles to increase their RCS to make them visible in radar sensing. It is worth to point out that, oceanographic bistatic applications, especially for ocean bistatic SAR [21, 22], is one of the most important application fields. Theoretical treatment is made on an assumed two scale model, that

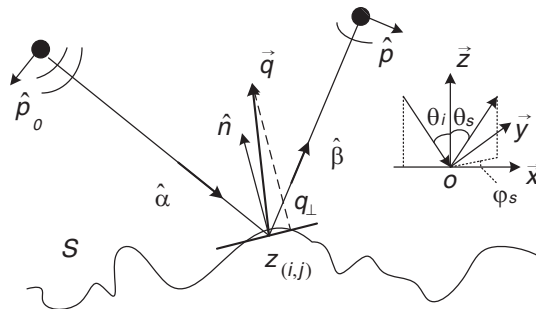


**Figure 2.** Geometry of a facet scattering surface.

is, treating the scattering sea surface as a combination of corrugations of two different scales. The problem is discussed on the Geometry of the scattering surface shown in Fig. 2. According to the two scale scattering model presented by Bass and Fuks [12, 17, 18], we get the scattering field in case of a dielectric rough surface and a plane incident wave.

$$\vec{E}_s = \frac{k^2 e^{ikR_s}}{\pi R_s} \vec{E}_0 \int_S F(\hat{p}_0, \hat{p}, \hat{\alpha}, \hat{\beta}, \hat{n}) \zeta(\vec{r}) \eta(\vec{r}, \hat{\alpha}, \hat{\beta}) e^{-i\vec{q}\cdot\vec{r}} d\vec{r} \quad (5)$$

Wherein most of symbols are defined under Fig. 2,  $\hat{p}_0, \hat{p}$  are the unit polarization vector;  $\hat{\alpha}$  is a unit vector directed from the transmitter, while  $\hat{\beta}$  is a unit vector directed to the reception point;  $\vec{q} = k(\hat{\beta} - \hat{\alpha})$ , and  $\epsilon$  indicates the permittivity of the dielectric surface;  $\hat{n}$  points in the normal direction to the surface  $S$ , that is,  $\hat{n} = -Z_x \hat{x} - Z_y \hat{y} + \hat{z} / \sqrt{1 + Z_x^2 + Z_y^2}$ ,  $Z_x, Z_y$  are the large scale slopes of each facet;  $\eta(\vec{r}, \hat{\alpha}, \hat{\beta})$  is for the possible shadowing of the surface  $S$  and may have two values 1 and 0 depending on whether the point  $r \in S$  is illuminated or not. The function  $F(\hat{p}_0, \hat{p}, \hat{\alpha}, \hat{\beta}, \hat{n})$  depends on the incident and scattering angle, different for the two polarizations, as well as the local normal unit of each facet; its detailed expression is derived in the Appendix A.

### 3.2. Slope-deterministic Facet Model (SDFM)

In the following context, we are only concerned with the surface contribution, while neglecting the multiple scattering totally. As a numerical method, the large-scale sea surface can be fit into approximately by sufficient small plane facets, centered on the grid points. Accordingly, some facets may be in a specular configuration, while others in a diffuse configuration. The scattering coefficient by near-specular facets can be computed under the geometric optics limit of the Kirchhoff approximation (KA-GO) [5]:

$$\sigma_{KA} = \pi k^2 q^2 |U_{pop}|^2 Prob/q_z^4 \quad (6)$$

where  $Prob$  is the Cox-Munk PDF [20].  $U_{pop}$  is polarization-dependent coefficients [5].

Since the scattering field in the bistatic formula of BFTSM is obtained in Eq. (5), in case of a plane incident wave, we can get:

$$\sigma_{TSM} = 4\pi R^2 \langle E_s E_s^* \rangle / A = 8k^4 \sigma^2 \langle F_{pop} F_{pop}^* \rangle W(q_{\perp}, \varphi) S(\theta_i, \theta_s) / A \quad (7)$$

where  $\sigma^2$  is the height variance of the small scale at resonant scattering wave number;  $q_{\perp}$  is the projection of the vector  $\vec{q}$  ( $\vec{q} = k(\hat{\beta} - \hat{\alpha})$ ) on to

the plane tangent at the point  $\vec{r}$  ( $r \in S$ ), and it is given by  $q_{\perp} = |\vec{q}| \sqrt{1 - (\hat{n} \cdot \vec{q}/|\vec{q}|)^2}$ ;  $W(k_x, k_y)$  is the two dimensional normalized ocean wave spectrum density and it is expressed in term of the capillary spectrum by  $\sigma^2 W(K, \varphi) = W_c(K, \varphi)/K$  [6],  $W_c(K, \varphi)$  is defined by Eq. (4). Thus, Eq. (7) can be rewritten by

$$\sigma_{TSM} = 8k^4 S(\theta_i, \theta_s) \langle F_{p0p} F_{p0p}^* \rangle W_c(K_l, \varphi)/K_l/A \quad (8)$$

where  $K_l$  ( $K_l = q_{\perp}$ ) is the water wave number for resonant scattering.  $S(\theta_i, \theta_s)$  is employed to evaluate the shadowing effect, which is discussed by Bourlier et al. [23] in detail. Therefore, from Eq. (8), it could be concluded that, the returns from different facets are proportional to the instantaneous Bragg Fourier components of the capillary spectrum, which leads to statistically independence.

Due to filter out the roughness components (some facets) for which the small perturbation method is inadequate, we ignore the wave number contribution by setting Eq. (8) to zero for  $K_l$  lower than the cut-off wave number  $k_d$ . It remains no unified guideline for the selection of the cutoff wave number  $k_d$ . Different authors make different choices, which range from Johnson et al. [24]  $k_d = k/2$ ; Brown [25]  $k_d = k/3$ ; Durden and Vesecky [26]  $k_d = k/5$ ; Jackson et al. [27]  $k_d = k/3$  to  $k_d = k/6$ ; Donelan and Pierson [28]  $k_d = k/40$ . A strong analysis is made by Hasselmann et al. [15]. They stated that the separation wave number  $k_d$  should be at least an order of magnitude smaller than the incident wave number. In order to satisfy the requirements of GO for the long-wave reflection field and the Bragg scattering theory, they restricted the  $k_d$  by  $0.05k \cos \theta_i \ll k_d \ll k \sin \theta_i$ , where  $\theta_i$  denotes the incident angle. In this regime, the dependence of the results on the choice of  $k_d$  is weak, so that the choice  $k_d = k/5$  was applied in their model. Soriano et al. [29] claimed that the dependence on the choice of  $k_d$  could be eliminated if the SPM is replaced by the first-order SSA in the two-scale combination. The influence of  $k_d$  on the BFTSM responsible for the Bragg scattering is discussed in Fig. 3. As one can see, at smaller cutoffs, the BFTSM term dominates more in the specular angles (smaller than  $20^\circ$ ). Here, we choose  $k_d = k/4$  empirically.

It has clear physical grounds to revise the TSM by a combination of KA with TSM contributions, rather than adding KA to SPM [26, 30]. Andreas et al. [30] released a “semi-deterministic” frame under which the facet context is locally characterized by the so-called “bistatic local angles” at a deterministic surface profile. They restrict the specular reflection zone with the local specular angles approximately below  $20^\circ$ , and introduce a weight factor to smooth the transition between the specular and diffuse region. Although the factor needs a theoretical

treatment of a more clear explain. Accordingly, we present a facet-based summation formula in which the elementary radar returns from respective facets are computed by the semi-deterministic scheme of combining geometric optics limit of the KA (KA-GO) with Bragg components of the extended BFTSM. It is quite similar to the scheme presented by Andreas et al.. In contrast, however, we relate the local configurations mainly to the sea slopes of the large scale profile and the Bragg-scattering part of the wave number spectrum. The implicit weight factor which is relevant to smooth the break point result by the region transition and the “local angle” division are not used. In order to apply the facet Bragg theory, the facet must be large in comparison with the wavelength of the incident radiation in the facet plane, and be sufficiently small as it can still be regarded as a plane [15]. We postulate the discrete facets are in proper size, so that the KA and TSM can be used in the local summation frame. In our treatment, the surface is generated by  $300 \times 300$  facets, and the respective resolution has been considered as  $1 \times 1$  meters. This is a statistical approach, and, experimentally, in the semi-deterministic diagram, the RCS average does not depend much upon the facet size [30]. Then, under a “semi-deterministic” scheme, the total scattering coefficient can be obtained by summing up returns from all the Bragg facets, including the non-Bragg contributions governed by Eq. (6):

$$\sigma_{\Sigma}^{p_0p} = \frac{S(\theta_i, \theta_s)}{A} \sum_{i=1}^M \sum_{j=1}^N \left[ 8k^4 F_{i,j}^{p_0p} F_{i,j}^{p_0p*} W_c(K_l, \varphi) / K_l + \pi k^2 q^2 \left| U_{i,j}^{p_0p} \right|^2 Prob/q_z^4 \right] \begin{matrix} Z y_{ij} = \{Z y_{ij} \in [\beta_{ij}]\} \\ Z x_{ij} = \{Z x_{ij} \in [\alpha_{ij}] | Z x_{ij} > -\cot \theta_i \} \end{matrix} \quad (9)$$

Due to avoid illuminating the rear of the tilted facets, the slopes

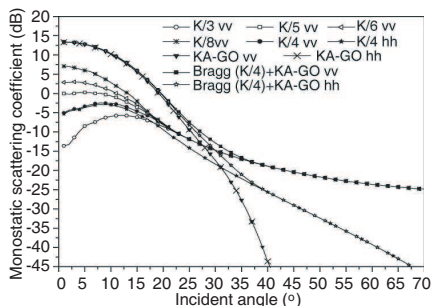


Figure 3. Analysis on cutoff wave number.

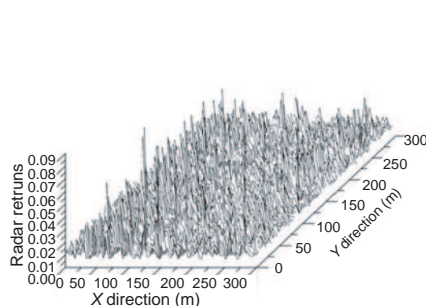
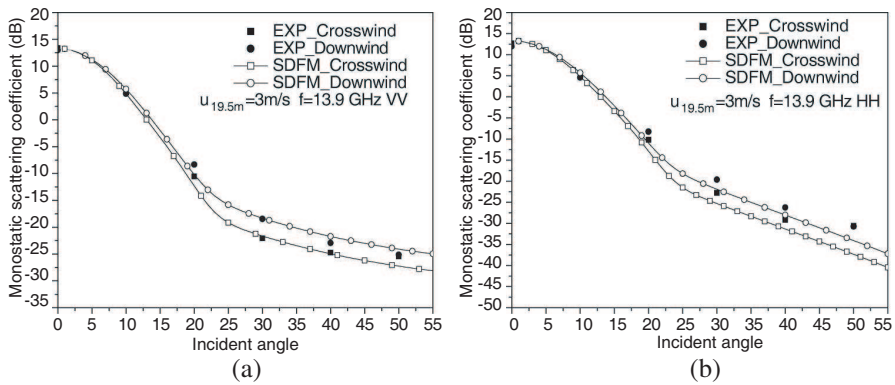


Figure 4. Simulated returns from individual facets.

along the  $x$  direction are limited above  $-\cot \theta_i$ .  $A$  is the area of the generated sea surface.

Under the facet scheme, the monostatic average varied with incident angles is obtained as a blend of KA-GO and  $k/4$  cutoff Bragg components of BFTSM (also see in Fig. 3), when the incident frequency is set to 14.0 GHz, for VV and HH polarizations. Fig. 4 displays the simulated returns from individual facets in the backscattering direction as the incident angle equals to  $40^\circ$ . Other parameters are fixed as: Wind direction: upwind; VV polarization; incident frequency: 14.0 GHz; wind speed: 5 m/s; sea simulation plot:  $300 \text{ m} \times 300 \text{ m}$ .



**Figure 5.** Experiment validation on impact of wind direction: (a) For VV polarization; (b) for HH polarization.

**Table 1.** The cost time on calculating the backscattering coefficient<sup>a</sup>.

Comparison Item	Generated sea model	HH polarization	VV polarization
CTSM	No need	333.687 s	410.343 s
SDFM	21.875 s	87.297 s	87.375 s

<sup>a</sup>The calculating parameters: a) Incident angle range:  $1^\circ \sim 89^\circ$ ,  $f = 14.0 \text{ GHz}$ ;  $u = 6.267 \text{ m/s}$ , sea area  $200 \times 200 \text{ m}^2$ , Upwind; b) computer capacity: Inter(R) Core(TM) 2 Quad CPU 2.50 GHz 2.49 GHz, 2.0 GB.

### 4. RESULTS ANALYSIS AND EXPERIMENTAL VALIDATION

Numerical validation is discussed on the basis of the experiment by W. L. JONES et al. in 1970s [31]. They had been measured the scattering signatures of the ocean over a range of surface wind speeds from 3 m/s to 23.6 m/s, typically wind directions and different polarizations. As the chosen spreading function can't describe the difference between downwind and upwind direction, the validation is only discussed in crosswind and downwind direction. Relative research on upwind/downwind asymmetry goes back to the literature on Modulation Transfer Function (MTF) presented by Romeiser et al. [32]. At a wind speed of 3 m/s, Figs. 5(a) and (b) show the comparisons with the measured data in VV and HH polarizations respectively. While in a wide range of sea states, from 3 m/s to 23.6 m/s, validation results are displayed in Fig. 6, (a) for VV polarization and (b) for HH polarization. From the numerical examples above, we find that our simulation is consistent with the experiment data well. In addition, high computational efficiency in our calculation on the backscattering coefficient could be observed, comparing with the conventional TSM (CTSM) [13], see in Table 1, in detail.

The bistatic configurations are discussed in Figs. 7 and 8. And the parameters are fixed as follows: The transmitter incident azimuth angle is equal to  $0^\circ$ , incident wave frequency is 14.0 GHz, the receiver azimuth is set to  $0^\circ$ , the receiver scattering angle is varied from  $-80^\circ$  to  $80^\circ$  and the wind direction is in downwind case. Fig. 7 shows the

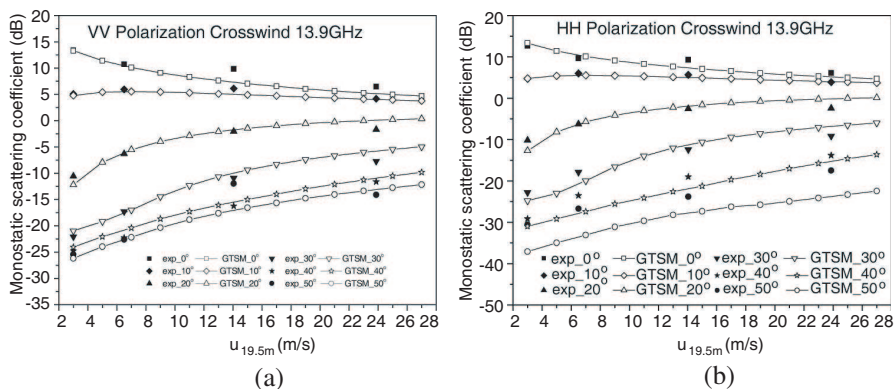


**Figure 6.** Experiment validation on impact of wind speed: (a) For VV polarization; (b) for HH polarization.

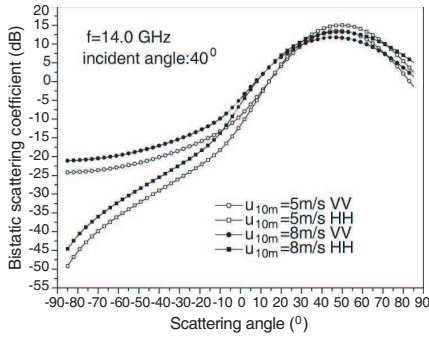


**Figure 7.** Simulated Bistatic NRCS.

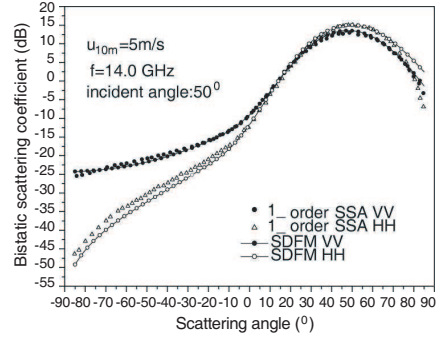


**Figure 8.** Comparison on SDFM with SSA1.

bistatic simulations by SDFM for two wind speeds, 5 m/s and 8 m/s, respectively, and the transmitter incident angle is  $40^\circ$ . As is apparent, the maximum energy is received around the specular direction  $40^\circ$ , and it decreases when the wind speed increases, which is a logical result. Fig. 8 compares the results yielded by the first order SSA [33] with SDFM for 5 m/s in HH and VV polarizations respectively, while the transmitter incident angle is  $50^\circ$ . It shows good agreement between SSA and SDFM, as the difference remains within about 2 dB.

## 5. CONCLUSION

A slope-deterministic facet model for the computation of the radar scattering cross section from the ocean-like surface is presented. As a numerical theory, it is a more comprehensive facet model which can reflect the specular and diffuse configurations, as well as the mono- and bistatic configurations. Combining all of these features under the facet-based frame may be outlined for the first time. Finally, the good agreement between the model results and available experimental data encourages us to employ the proposed model for further investigations on bistatic realistic SAR imagery simulations of marine scene.

## ACKNOWLEDGMENT

The authors thank the National Nature Science Foundation of China under Grant No. 60871070, the National Pre-research Foundation and the Foundation of the National Electromagnetic Scattering Laboratory for supporting this research.

### APPENDIX A.

As defined under the geometry in Fig. 2, the related parameters can be denoted as follows:

$$\begin{aligned}\hat{\alpha} &= \sin \theta_i \cos \varphi_i \hat{x} + \sin \theta_i \sin \varphi_i \hat{y} - \cos \theta_i \hat{z} \\ \hat{\beta} &= \sin \theta_s \cos \varphi_s \hat{x} + \sin \theta_s \sin \varphi_s \hat{y} + \cos \theta_s \hat{z} \\ \hat{p}_{0h} &= -\sin \varphi_i \hat{x} + \cos \varphi_i \hat{y} \\ \hat{p}_{0v} &= -\cos \theta_i \cos \varphi_i \hat{x} - \cos \theta_i \sin \varphi_i \hat{y} - \sin \theta_i \hat{z} \\ \hat{p}_h &= -\sin \varphi_s \hat{x} + \cos \varphi_s \hat{y} \\ \hat{p}_v &= \cos \theta_s \cos \varphi_s \hat{x} + \cos \theta_s \sin \varphi_s \hat{y} - \sin \theta_s \hat{z}\end{aligned}$$

Then, the function  $F(\hat{p}_0, \hat{p}, \hat{\alpha}, \hat{\beta}, \hat{n})$  can be expressed as:

$$\begin{aligned}F_{p_0p} &= \frac{aa_0(1-\varepsilon)}{(b+a\varepsilon)(b_0+a_0\varepsilon)} \left\{ \frac{\varepsilon-1}{a+b} \left[ \hat{\beta} \times (\hat{n} \times \hat{p}_0) \right] \right. \\ &+ \frac{\varepsilon-1}{a_0+b_0} \left[ \hat{\beta} \times (\hat{\beta} \times (\hat{n} \times (\hat{\alpha} \times \hat{p}_0))) \right] \\ &+ \frac{(\varepsilon-1)^2}{(a+b)(a_0+b_0)} \left[ \hat{\beta} \times (\hat{n} \times (\hat{n} \times (\hat{\alpha} \times \hat{p}_0))) \right] \\ &\left. + (\varepsilon-1)(\hat{n} \cdot \hat{p}_0) \left[ \hat{\beta} \times (\hat{\beta} \times \hat{n}) \right] + \left[ \hat{\beta} \times (\hat{\beta} \times \hat{p}_0) \right] \right\} \\ &= \frac{aa_0(1-\varepsilon)}{(b+a\varepsilon)(b_0+a_0\varepsilon)} \left\{ \frac{\varepsilon-1}{a+b} \left[ (\hat{\beta} \cdot \hat{p}_0)(\hat{n} \cdot \hat{p}) - (\hat{p}_0 \cdot \hat{p}) - a(\hat{p}_0 \cdot \hat{p}) \right] \right. \\ &- (\varepsilon-1)(\hat{n} \cdot \hat{p}_0)(\hat{n} \cdot \hat{p}) + \frac{(\varepsilon-1)^2}{(a+b)(a_0+b_0)} \left[ (\hat{\alpha} \cdot \hat{\beta})(\hat{n} \cdot \hat{p}_0)(\hat{n} \cdot \hat{p}) \right. \\ &\left. \left. - a(\hat{\alpha} \cdot \hat{p}) + a_0(\hat{\beta} \cdot \hat{p}_0)(\hat{n} \cdot \hat{p}) - aa_0(\hat{p}_0 \cdot \hat{p}) \right] \right\} \quad (A1)\end{aligned}$$

where,  $a_0 = \cos \theta_i$ ,  $b_0 = \sqrt{\varepsilon - \sin^2 \theta_i}$ ,  $a = \hat{n} \cdot \hat{\beta}$ ,  $b = \sqrt{\varepsilon - 1 + a^2}$ .

For the sake of brevity, Let  $d = 1/\sqrt{1 + Zx^2 + Zy^2}$ ,  $A_{p_0p} = \hat{p}_0 \cdot \hat{p}$ ,  $B_{p_0p} = (\hat{n} \cdot \hat{p}_0)(\hat{n} \cdot \hat{p})$ ,  $C_{p_0p} = (\hat{\beta} \cdot \hat{p}_0)(\hat{n} \cdot \hat{p})$ ,  $D_{p_0p} = (\hat{n} \cdot \hat{p}_0)(\hat{\alpha} \cdot \hat{p})$ ,  $Q_{p_0p} = (\hat{\alpha} \cdot \hat{\beta})B_{p_0p} - a(\hat{\alpha} \cdot \hat{p})$ , then,  $\hat{n} = d(-Z_x \hat{x} - Z_y \hat{y} + \hat{z})$ , and Eq. (A1) can be simplified:

$$\begin{aligned}F_{p_0p} &= \frac{aa_0(1-\varepsilon)}{(b+a\varepsilon)(b_0+a_0\varepsilon)} \left\{ \frac{\varepsilon-1}{a+b} [C_{p_0p} - aA_{p_0p}] - A_{p_0p} - (\varepsilon-1)B_{p_0p} \right. \\ &\left. + \frac{(\varepsilon-1)^2}{(a+b)(a_0+b_0)} [Q_{p_0p} + a_0C_{p_0p} - aa_0A_{p_0p}] + \frac{1-\varepsilon}{a_0+b_0} [D_{p_0p} + a_0A_{p_0p}] \right\} \quad (A2)\end{aligned}$$

$$\begin{aligned}
A_{vv} &= \cos \theta_i \cos \varphi_i \cos \theta_s \cos \varphi_s + \cos \theta_i \sin \varphi_i \cos \theta_s \sin \varphi_s - \sin \theta_i \sin \theta_s \\
B_{vv} &= -d^2 (Zx \cos \theta_i \cos \varphi_i + Zy \cos \theta_i \sin \varphi_i - \sin \theta_i) \\
&\times (-Zx \cos \theta_s \cos \varphi_s - Zy \cos \theta_s \sin \varphi_s - \sin \theta_s) \\
C_{vv} &= -d (-Zx \cos \theta_s \cos \varphi_s - Zy \cos \theta_s \sin \varphi_s - \sin \theta_s) \\
&\times (-\cos \theta_i \cos \varphi_i \sin \theta_s \cos \varphi_s - \cos \theta_i \sin \varphi_i \sin \theta_s \sin \varphi_s - \sin \theta_i \cos \theta_s) \\
D_{vv} &= -d (Zx \cos \theta_i \cos \varphi_i + Zy \cos \theta_i \sin \varphi_i - \sin \theta_i) \\
&\times (\sin \theta_i \cos \varphi_i \cos \theta_s \cos \varphi_s + \sin \theta_i \sin \varphi_i \cos \theta_s \sin \varphi_s + \cos \theta_i \sin \theta_s) \\
Q_{vv} &= -B_{vv} (\sin \theta_i \cos \varphi_i \sin \theta_s \cos \varphi_s + \sin \theta_i \sin \varphi_i \sin \theta_s \sin \varphi_s \\
&- \cos \theta_i \cos \theta_s) + a (\sin \theta_i \cos \varphi_i \cos \theta_s \cos \varphi_s + \sin \theta_i \sin \varphi_i \cos \theta_s \sin \varphi_s \\
&- \cos \theta_i \sin \theta_s) \\
A_{hh} &= -\cos \varphi_i \cos \varphi_s - \sin \varphi_i \sin \varphi_s \\
B_{hh} &= -d^2 (Zx \sin \varphi_i - Zy \cos \varphi_i) (Zx \sin \varphi_s - Zy \cos \varphi_s) \\
C_{hh} &= -d (Zx \sin \varphi_s - Zy \cos \varphi_s) (-\sin \varphi_i \sin \theta_s \cos \varphi_s + \cos \varphi_i \sin \theta_s \sin \varphi_s) \\
D_{hh} &= -d (Zx \sin \varphi_i - Zy \cos \varphi_i) (-\sin \theta_i \cos \varphi_i \sin \varphi_s + \sin \theta_i \sin \varphi_i \cos \varphi_s) \\
Q_{hh} &= -B_{hh} (\sin \theta_i \cos \varphi_i \sin \theta_s \cos \varphi_s + \sin \theta_i \sin \varphi_i \sin \theta_s \sin \varphi_s \\
&- \cos \theta_i \cos \theta_s) + a (\sin \theta_i \sin \varphi_i \cos \varphi_s - \sin \theta_i \cos \varphi_i \sin \varphi_s)
\end{aligned}$$

Similarly, the parameters above can be obtained for cross polarizations.

## REFERENCES

1. Franceschetti, G., M. Migliaccio, and D. Riccio, "On ocean SAR raw signal simulation," *IEEE Trans. Geosci. Remote Sens.*, Vol. 36, No. 1, 84–100, 1998.
2. Kasilingam, D. P. and O. H. Shemdin, "Models for synthetic aperture radar imaging of the ocean: A comparison," *J. Geophys. Res.*, Vol. 95, 16263–16276, 1990.
3. Franceschetti, G., A. Iodice, D. Riccio, G. Ruello, and R. Siviero, "SAR raw signal simulation of oil slicks in ocean environments," *IEEE Trans. Geosci. Remote Sens.*, Vol. 40, No. 9, 1935–1949, 2002.
4. Beckmann, P. and A. Spizzichino, *The Scattering of Electromagnetic Waves from Rough Surfaces*, Macmillan, New York, 1963.
5. Ulaby, F. T., R. K. Moore, and A. K. Fung, *Microwave Remote Sensing: Active and Passive*, Vol. 2, Artech House, Norwood, MA, 1986.
6. Chan, H. L. and A. K. Fung, "A theory of sea scatter at large incident angles," *J. Geophys. Res.*, Vol. 82, 3439–3444, 1977.

7. Voronovich, A. G., "Small-slope approximation for electromagnetic wave scattering at a rough interface of two dielectric half-spaces," *Waves Random Media*, Vol. 4, 337–367, 1994.
8. Shaw, W. T. and A. J. Dougan, "Green's function refinement as an approach to radar backscatter: General theory and application to LGA scattering from the ocean," *IEEE Trans. Antennas Propag.*, Vol. 46, 57–66, 1998.
9. Guo, L. and Z. Wu, "Application of the extended boundary condition method to electromagnetic scattering from rough dielectric fractal sea surface," *Journal of Electromagnetic Waves and Applications*, Vol. 18, No. 9, 1219–1234, 2004.
10. Nedlin, G. M., S. R. Chubb, and A. L. Cooper, "The integral equation method for electromagnetic scattering from the ocean: Beyond a perfect conductor model," *Radio Sci.*, Vol. 34, No. 1, 27–49, 1999.
11. Valenzuela, G. R., "Theories for the interaction of electromagnetic waves and oceanic waves: A review," *Bound. Layer Met.*, Vol. 13, 61–85, 1978.
12. Bass, F. G. and I. M. Fuks, *Wave Scattering from Statistically Rough Surfaces*, 418–442, Pergamon Press Oxford, New York, 1979.
13. Fung, A. K. and K. Lee, "A semi-empirical sea-spectrum model for scattering coefficient estimation," *IEEE J. Oceanic Engineering*, Vol. 7, No. 4, 166–176, 1982.
14. Franceschetti, G., M. Migliaccio, D. Riccio, and G. Schirinzi, "SARAS: A synthetic aperture radar (SAR) raw signal simulator," *IEEE Trans. Geosci. Remote Sens.*, Vol. 30, No. 1, 110–123, 1992.
15. Hasselman, K., et al., "Theory of synthetic aperture radar ocean imaging: A MARSEN view," *J. Geophys. Res.*, Vol. 90, 4659–4686, 1985.
16. West, J. C., R. K. Moore, and J. C. Holtzman, "The slightly-rough facet model in radar imaging of the ocean surface," *Int. J. Remote Sens.*, Vol. 11, No. 4, 617–637, 1990.
17. Fuks, I. M., "Theory of radio wave scattering at a rough sea surface," *Radiophysics and Quantum Electronics*, Vol. 9, No. 5, 513–519, 1966.
18. Bass, F. G., I. M. Fuks, et al., "Very high frequency radiowave scattering by a disturbed sea surface," *IEEE Trans. Antennas Propagat.*, Vol. 16, No. 5, 554–568, 1968.
19. Joung, S. and J. Shelton, "3 Dimensional ocean wave model using directional wave spectra for limited capacity computers,"

- IEEE OCEANS '91. Ocean Technologies and Opportunities in the Pacific for the 90's. Proceedings.*, Vol. 1, 608–614, 1991.
20. Cox, C. and W. H. Munk, "Statistics of the sea surface derived from sun glitter," *J. Marine Res.*, Vol. 13, 198–227, 1954.
  21. Moccia, A., G. Rufino, and M. D. Luca, "Oceanographic applications of spaceborne bistatic SAR," *IEEE International Geoscience and Remote Sensing Symposium, IGARSS'03. Proceedings.*, Vol. 3 No. 21–25, 1452–1454, 2003.
  22. Kassem, M. J. B., J. Saillard, and A. Khenchaf, "BISAR mapping I. Theory and modelling," *Progress In Electromagnetics Research, PIER* 61, 39–65, 2006.
  23. Bourlier, C., G. Berginc, and J. Saillard, "One and two-dimensional stationary shadowing functions for any height and slope stationary uncorrelated surface in the monostatic and bistatic configurations," *IEEE Trans. Antennas Propagat.*, Vol. 50, No. 3, 312–324, 2002.
  24. Johnson, J. T., R. T. Shinan, and J. A. Kong, "A numerical study of the composite surface model for ocean backscattering," *IEEE Trans. Geosci. Remote Sens.*, Vol. 36, 72–83, 1998.
  25. Brown, G. S., "Backscattering from a Gaussian-distributed, perfectly conducting rough surface," *IEEE Trans. Antennas Propagat.*, Vol. 26, 472–482, 1978.
  26. Durden, S. L. and J. F. Vesecky, "A physical radar cross-section model for a wind-driven sea with swell," *IEEE J. Oceanic Engineering*, Vol. 10, 445–451, 1985.
  27. Jackson, F. C., W. T. Walton, and D. E. Hines, "Sea surface mean square slope from Ku-band backscatter data," *J. Geophys. Res.*, Vol. 11, 411–427, 1997.
  28. Donelan, M. A. and W. J. Pierson, "Radar scattering and equilibrium ranges in wind-generated waves with application to scatterometry," *J. Geophys. Res.*, Vol. 92, 4971–5029, 1987.
  29. Soriano, G. and C. A. Guerin, "A cutoff invariant two-scale model in electromagnetic scattering from sea surfaces," *IEEE Trans. Geosci. Remote Sens.*, Vol. 5, 199–203, 2008.
  30. Andreas, A. B., A. Khenchaf, and A. Martin, "Bistatic radar imaging of the marine environment Part I: Theoretical background," *IEEE Trans. Geosci. Remote Sens.*, Vol. 45, No. 11, 3372–3383, 2007.
  31. Jones, W. L., L. C. Schroeder, and J. L. Mitchell, "Aircraft measurements of the microwave scattering signature of the ocean," *IEEE Trans. Antennas Propagat.*, Vol. 25, No. 1, 52–61, 1977.

32. Romeiser, R., W. Alpers, and V. Wismann, "An improved composite surface model for the radar backscattering cross section of the ocean surface 1. Theory of the model and optimization/validation by scatterometer data," *J. Geophys. Res.*, Vol. 102, 25237–25250, 1997.
33. Awada, A., M. Y. Ayari, A. Khenchaf, and A. Coatanhay, "Bistatic scattering from an anisotropic sea surface: Numerical comparison between the first-order SSA and the TSM models," *Waves in Random and Complex Media*, Vol. 16, No. 3, 383–394, 2006.